Climate effects of a hypothetical regional nuclear war: Sensitivity to emission duration and particle composition

Francesco S.R. Pausata[1,*†], Jenny Lindvall[1†], Annica M. L. Ekman[1] and Gunilla Svensson[1]

Affiliation

[1]*Department of Meteorology, Stockholm University and Bolin Centre for Climate Research, Stockholm, Sweden*

**Correspondence to: francesco.pausata@misu.su.se*

[†]*The authors have equally contributed to the manuscript*

Abstract

Here we use a coupled atmospheric-ocean-aerosol model to investigate the plume development and climate effects of the smoke generated by fires following a regional nuclear war between emerging third-world nuclear powers. We simulate a standard scenario where 5 Tg of black carbon (BC) is emitted over 1 day in the upper troposphere-lower stratosphere. However, it is likely that the emissions from the fires ignited by bomb detonations include a substantial amount of particulate organic matter (POM) and that they last more than 1 day. We therefore test the sensitivity of the aerosol plume and climate system to the BC/ POM ratio (1:3, 1:9) and to the emission length (1 day, 1 week, 1 month). We find that in general, an emission length of 1 month substantially reduces the cooling compared to the 1-day case, whereas taking into account POM emissions notably increases the cooling and the reduction of precipitation associated with the nuclear war during the first year following the detonation. Accounting for POM emissions increases the particle size in the short-emission-length scenarios (1 day/1 week), reducing the residence time of the injected particle. While the initial cooling is more intense when including POM emission, the long-lasting effects, while still large, may be less extreme compared to the BC-only case. Our study highlights that the emission altitude reached by the plume is sensitive to both the particle type emitted by the fires and the emission duration. Consequently, the climate effects of a nuclear war are strongly dependent on these parameters.

This article has been accepted for publication and undergone full peer review but has not been through the copyediting, typesetting, pagination and proofreading process, which may lead to differences between this version and the Version of Record. Please cite this article as doi: eft2.2016EF000415

1 Introduction

The current risk of global nuclear war seems less pressing than 30 years ago as the global nuclear arsenal has declined by more than a factor of three over these years. Nevertheless, society is still facing a potential nuclear disaster owing to the proliferation of small nuclear powers, which may lead to a regional nuclear conflict. Besides the rather well-known immediate consequences of a nuclear weapon explosion, there are more uncertainties related to the subsequent widespread fires, including the aerosol particle emission amount, the emission composition and duration**.** These particles are assumed to be immediately lifted by the fires to the upper troposphere/lower stratosphere region where they will reflect and absorb solar radiation, locally heating the atmosphere and cooling the surface. The first studies using global climate models (GCMs) to examine the impact of the particles (e.g. *Turco et al.* [1983]) showed catastrophic climatic consequences of a nuclear war between superpowers, with subfreezing land temperatures even during summer. More recent studies, using state-of-the-art global climate models, have assessed the damage that might result from a more restrictive use of nuclear weapons [*Robock et al.*, 2007; *Toon et al.*, 2007a, 2007b; *Mills et al.*, 2008; *Stenke et al.*, 2013]. These studies assume that a regional conflict over India/Pakistan involving 50 Hiroshima-size bombs could generate up to 5 Tg of black carbon (BC) in the upper-troposphere/lower stratosphere after an initial 20% removal as "black rain" [*Toon et al.*, 2007a]. Even for such a scenario, the effects of the particles on the solar radiation would lead to colder and drier conditions for years after the conflict [*Robock et al.*, 2007; *Toon et al.*, 2007a], together with enhanced ultraviolet radiation owing to massive ozone destruction [*Mills et al.*, 2008]. Using a GCM, Robock et al. (2007) estimated that such a BC injection reduces the global-average surface short-wave radiation by a maximum of about 16 W m^{-2} (after about five months) and decreases the global mean surface temperature by 1.3°C. The BC injection also modifies the precipitation associated with the Asian summer monsoon. All changes have devastating impacts on the agriculture productivity in regions far from the conflict [*Toon et al.*, 2007b; *Özdoğan et al.*, 2013; *Xia and Robock*, 2013; *Mills et al.*, 2014; *Xia et al.*, 2015].

All previous reported GCM studies have, however, injected the 5 Tg of BC over 1 day or 1 model time step and have not included any other particles than BC such as organic carbon (OC) that can be over 10 times larger in amount compared to BC during for example forest fires [*Liu et al.*, 2014]. To put the magnitude of the estimated emissions in perspective, the entire global annual emission from all sources (from fossil fuel combustions to forest fires) is estimated to be around ~8 Tg for BC and ~34 Tg for OC, with an uncertainty ranges of 4-22 Tg and 17-77 Tg respectively [*Bond et al.*, 2004]. Corroborating these results, *Liu et al.* [2014] showed that fire smoke particles are composed of approximately 5%–10% (by mass) BC as compared to about 50%–70% OC. *May et al.* [2014] analyzed a large number of different smoke plumes in the laboratory and for prescribed fires in the US, and found a range of BC and particulate organic matter - POM (i.e. the sum of OC and associated chemical elements) emission ratios depending on fuel type, fuel composition and combustion conditions (see Table 4 in *May et al.* [2014]). However, in most samples, POM typically dominates the sub-micron aerosol particle composition. Therefore, it is highly probable that the particle emissions from the fires also include a significant amount of OC; the bomb explosions are likely capable of igniting not only the urban areas but also the vegetated parts within and surrounding the cities, including a variable mix of vegetation and different types of fuels. OC has different optical properties compared to BC: while BC particles absorb sunlight and reduce the planetary albedo, OC particles have a much lower absorption coefficient and generally scatter solar radiation. When co-emitted OC can coagulate with BC, increasing BC absorption by ~50% [*Toon and Farlow*, 1981; *Toon et al.*, 2007b]. However, BC/OC coagulation also leads to a larger particle size, which most likely will reduce the residence time of the particles. Hence, if OC is co-emitted with the BC particles, the aerosol particle scattering and absorption will be affected and consequently the self-lofting capacity of the fire plumes into the stratosphere and potentially the mesosphere. Therefore, it is important to investigate the impact of co-emissions of OC and BC on the fire plume height development and climate impacts that may differ from previous studies, which only BC emissions have been considered (e.g., *Robock et al.* [2007]; *Stenke et al.* [2013]; *Mills et*

al. [2014]).

It is plausible that the large fires caused by 50 Hiroshima-size bombs may last longer than 1 day, or just one time step, as assumed in previous studies. Furthermore, it is also feasible that multiple bomb detonations occur at different times over the course of a week or a month. Therefore, it is relevant to test the sensitivity of the climate system to both co-emissions of BC and OC, and the emission duration.

In this study, we use a coupled aerosol-atmosphere-ocean model (NorESM1-M) to run several sensitivity tests in which we explore the importance of some of the emission assumptions described above, including different BC/POM ratio and varying the emission duration of a hypothetical regional nuclear war between India and Pakistan. In doing so, we investigate the impacts of these changes on (a) the atmospheric thermal gradient and subsequent lofting of the particles, gaining insight on the importance of such assumptions for the stratospheric warming and lofting of BC; and (b) the surface climate in terms of precipitation and temperature.

The paper is structured as follows. In Section 2 we provide a description of the coupled GCM used and the experimental set-up adopted to simulate the regional nuclear war. In Section 3 we investigate the effect of applying different BC/POM emission ratios and emission duration, as well as the simulated short-term (1 year) and long-term (up to 10 years) impacts on surface climate and the growing season following the nuclear bomb detonations. Discussion and conclusions are provided in Section 4.

2 Methods

2.1 Climate model

The simulations were conducted using the coupled atmospheric-ocean-aerosol model NorESM1-M [*Bentsen et al.*, 2013; *Iversen et al.*, 2013]. NorESM1-M is an Earth System Model that for the atmospheric part of the model uses a modified version of the Community Atmospheric Model version 4 (CAM4, *Neale et al.*, [2013]) – CAM4–Oslo [*Kirkevåg et al.*, 2013]. The modifications include an updated aerosol model with online calculation of aerosol particles and

their direct effect on radiation, as well as parameterizations of the first and second indirect effects of aerosol particles on warm clouds. The aerosol model includes the life cycle of sea salt, mineral dust, particulate sulfate, black carbon and POM. All particles at all levels are subject to gravitational settling, which is an important removal process for particles at high altitudes. The wet deposition of aerosol particles in the model is directly coupled to the simulated precipitation rates, including precipitation from convection. The washout takes into account the aerosol size, composition and mixing state; i.e. hydrophilic aerosols (e.g., sulfate) are removed more easily than hydrophobic aerosols (e.g., BC). In NorESM1-M, BC and POM are allowed to coagulate and also become coated with sulfate, organics, and other light-scattering material. In our experiments, we used the default values of optical properties for BC and POM in NorESM1-M, and we assume an initial effective radius of about 0.1 μm or BC and 0.4 μm for POM (see Table 1 in Kirkevåg et al. [2013]). Previous studies have used an effective radius for BC ranging between 0.05 and 0.1 μm [*Robock et al.*, 2007; *Mills et al.*, 2014]. We inject POM to account for the OC emissions that will occur during the fires. The POM/OC ratio typically ranges between 1.4 for fossil fuel and 2.6 for biomass burning emissions [*Turpin and Lim*, 2001; *Kirkevåg et al.*, 2013]. Therefore, OC emissions correspond to roughly 50-80% of the POM injected. A detailed description of the aerosol representation, aerosol-radiation and aerosol-cloud interactions as well as the initial modal size parameters can be found in Kirkevåg et al. [2013].

CAM4–Oslo uses the finite volume dynamical core for transport calculations, with horizontal resolution 1.9° (latitude) × 2.5° (longitude) and 26 vertical levels (model top 3 hPa, ~40-45 km), as in the original CAM4. CAM4–Oslo is coupled with the updated version of the Miami Isopycnic Coordinate Ocean Model – MICOM [*Assmann et al.*, 2010]. The sea ice and land models are the same as in the Community Climate System Model version 4 (CCSM4, Gent et al. [2011]).

The model adequately represents the modern climate variability; a detailed analysis of the NorESM1-M performance is provided in Iversen et al. [2013]. The model has also been used to simulate the transport and removal of sulfate aerosols during high-latitude volcanic eruptions and

has shown good performance in simulating the residence time of the volcanic aerosols [*Pausata et al.*, 2015a].

2.2 Experiment set-up

We generate ensembles composed of 5 to 10 one-year members, assuming different amounts of BC and POM (Table 1). In each experiment, we have injected 5 Tg of BC together with either 0, 15 or 45 Tg of POM. The BC-only case has been chosen as comparison to previous studies, 1:3 and 1:9 BC/POM ratio (i.e. approximately 1:1.5 and 1:4.5 BC/OC ratio, respectively) ratios have been chosen to account for organic carbon emissions, which can be larger than BC emissions during fires. The 1:9 BC/POM ratio is assumed to be representative of spreading fires to the surrounding vegetated areas and hence, a mix of fossil fuel and biomass burning. The 1:3 ratio instead is a more conservative estimate assuming that the fuel for the fires are confined to the urban areas and the spreading is limited.

The choice of the BC/POM ratios must be considered rather arbitrary given the very wide range of possible BC/POM ratios observed during different type of fires (e.g., *May et al.* [2014]). An estimate of burnable organic material for Pakistan and India is not available. Nevertheless, organic carbon is ubiquitous and during the hypothetical city fires the organic matter would come not only from trees or other vegetated areas (inside and outside the cities) but also from wooden buildings, car tires, dung, and so on. Even in the BC emission estimate based on an investigation of available combustible mass loadings in Indian and Pakistan cities that will produce the 6 Tg of BC (5 Tg after "black rain" removal) [*Toon et al.*, 2007a], there is probably at least 1-2 Tg of POM.

In our model simulations, the particles are, as in previous studies, injected uniformly into the upper troposphere (300–150 hPa) over 50 grid-points (for a total area of 10° latitude x 25° longitude) centered above India and Pakistan (Table 1), using variable emission durations (1 day; 1 week; and 1 month) starting on January 1st. The length of the fire emissions has been chosen to reproduce previous studies (1 day) as well as to test the hypothesis of long-lasting fires, in case the fires spread to the surrounding vegetated areas. The choice of 1 week or 1 month is arbitrary.

We select a specific year (1986) taken from a transient 155-year simulation (1850-2005) and we use the initial conditions of the days preceding or following the date of the assumed detonation to perturb the model initial state (on January 1st) to generate the ensemble members. The selected year is characterized by a neutral ENSO state to avoid possible ENSO imprint on the simulated climate anomalies associated with the nuclear war [*Pausata et al.*, 2015a]. The choice of the detonation date (January 1st) is arbitrary and follows [*Mills et al.*, 2014]. The choice is further driven by the fact that the high concentrations of BC and POM tend to render the model unstable during the summer months. For some experiments, we were not able to perform more than five members because of the model instability; while for others the aim of ten members was reached (see Table 1).

In a similar manner, we generate an equivalent reference ensemble consisting of 20 members with BC and POM set to background conditions to get an estimate of the model's natural variability to be compared with the change signal obtained in the emission experiments. Historical emissions for the aerosol concentrations are taken from IPCC CMIP5 protocol, see Kirkevåg et al. (2013).

The ensembles are run for one year to test how the initial lofting of particles is affected by co-emissions of BC and OC and emission duration. In addition, for one case in which both BC and POM are injected over a week ($5BC/15POM_{1w}$), we have extended the simulation to 10 years, in order to compare this long-term response to the well-studied case of BC-only emissions presented in *Robock et al.* [2007] and *Mills et al.* [2014].

3 Results

In this section, we first compare how the different assumptions of the BC/POM ratio and emission length affect the distribution and the burden of the injected particles. We thereafter present the impacts of such assumptions on the short-term (1 year) net radiative imbalance at the surface, and on global near surface temperature and precipitation; we also compare our results with previously reported modeling studies. Finally, we select the experimental setup with the intermediate BC/POM ratio emission length, and discuss the long term effects (up to 10 years) on the surface climate and growing season following the nuclear bomb detonations.

3.1 Simulated particle distribution and burden

In the standard case ($5BC_{1d}$) experiment, most of the BC aerosol is carried well above the tropopause since the aerosol particles absorb SW radiation, heat the ambient air, and hence induce self-lofting, consistent with previous studies [*Robock et al.*, 2007; *Mills et al.*, 2008, 2014]. The maximum peak mass mixing ratio of about 20 kg (BC)/10^9 kg (air), reaches the top of the model at ~40 km within one month and then sinks down to 25 km after 10-12 months (Fig. 1a). These values are notably lower compared to the values shown in a recent work by Mills et al. (2014) where the BC peak is around 60 kg (BC)/10^9 kg (air) reaching heights of up to 60 km a.s.l. The maximum peak stays in the upper stratosphere (~40-50 km) for the entire first year. We surmise that the reduced lofting and the faster sinking are likely due to the lower top of the atmosphere and vertical resolution in NorESM1-M compared to Mills et al. (2014) that used CESM1 (WACCAM) with 66 vertical levels and a model top of ~145 km. Earlier studies, that have used models with coarser resolution and lower model top [*Robock et al.*, 2007; *Mills et al.*, 2008], also show less lifting. On the other hand, the BC removal is in agreement with previous studies [*Robock et al.*, 2007; *Mills et al.*, 2008, 2014], showing that within the first four months about 1.5 Tg of BC is removed, half of which occur in the first few weeks due to rainout as the plume initially partly is in the troposphere (Fig. 1). After one year, the remaining BC burden is around 3.2 Tg compared to ~3.4-3.6 Tg in the previous studies. Our results suggest that the low model top is limiting the BC lofting in the $5BC_{1d}$ scenario but does not largely affect the residence time. The reason may be due to compensating errors as the low model top confines the aerosol particles below 35-40 km and a relatively weak stratospheric circulation prolongs the aerosol residence time (not shown). These compensating errors result in a similar particle residence time as in high-top models, which allows for a comparison of the simulated climate effects with previous studies.

The absorption of shortwave radiation by the BC particles leads to stratospheric warming of up to 45°C compared to the reference case (Fig 1a). The maximum temperature anomaly is larger in the study by *Mills et al.* [2014] who also found the peak anomaly at a height above the model top in

our experiments. However, there is little air at these heights so it is easily heated. The temperature change in our experiment is indeed comparable with *Mills et al.* [2014] at the 10 hPa pressure level.

When the 5 Tg of BC are evenly released during a week ($5BC_{1w}$) or a month ($5BC_{1m}$), the maximum peak in the mass mixing ratios is notably lower than in the $5BC_{1d}$ experiment and is reached after 4-5 months (Fig. 1b, c). In the $5BC_{1w}$ experiment, a maximum of 10 kg (BC)/10^9 kg (air) is centered around 20-25 km, whereas a maximum of only ~5 kg (BC)/10^9 kg (air) is confined in the lower stratosphere at around 15 km in the $5BC_{1m}$ experiment. The length of the emission affects the BC density in the atmosphere and leads to a decreased heating and consequently a reduced lofting as the emission duration increases.

Similar behavior of the plume development is found in the BC+POM experiments (Fig. 1 d-f): The increased emission duration causes a lower maximum of BC particle mixing ratios compared to the 1d case. The POM mixing ratios follow the same pattern as the BC mixing ratios (not shown); however, to ease the comparison between the BC and BC+POM cases we have displayed only the BC mixing ratios.

The additional POM injection leads to a stronger warming of the middle stratosphere (around 10-30 hPa) compared to the BC case (Fig. 1), which is most likely due to an increased absorption associated with BC/POM coagulation [Toon and Ackerman, 1981; Toon et al., 2007b]; however, the associated larger particle size reduces the residence time and lowers the maximum particle mixing ratios in the 1-day and 1-week experiments compared to the BC-only case (Figs. 1 and 2a). In the 1-month scenario, instead, the BC/POM coagulation is less efficient – given the slow release – and therefore, the difference in particle size between the BC-only and BC+POM cases is most likely negligible. The increased absorption, on the other hand, is the dominant effect. This leads to a larger warming in the BC+POM case (Fig. 1c and f) and hence stronger lifting and longer residence time compared to the BC-only case (Fig. 2a).

In summary, the emission duration and the type of particles injected are very important in determining the net lofting of the injected aerosol. Our results show that only when the emissions

occur over 1 day, the particles' concentration maxima are located at the very top of the model (~40-45 km) and hence would potentially be located well above the stratosphere (>50-55 km). On the other hand, when extending the emission length to a week or more the maximum of the particle mixing ratio is well within the middle-lower stratosphere.

The globally averaged BC mass burden after one month from the start of the injection is similar in all experiments with values around 4 Tg (Fig. 2a), given that the wet deposition in the first month plays a minor role due to the injection height in the upper troposphere and the detonation time occurring during the dry monsoon season. The estimated BC emissions (5 Tg) already take into account the initial rain-out as "black-rain" as described in detail in *Toon et al.* [2007a]. After the initial month, the distribution of the BC particles in the atmosphere is substantially affected by the different injection duration (Fig. 1).

After twelve months from the start of the injection, the stronger BC removal in the $5BC_{1m}$ results in ~1 Tg less of BC compared to $5BC_{1w}$ and $5BC_{1d}$, since the lower level of BC lofting causes faster fallout (Fig. 2a).

3.2 Simulated global short-term radiative balance, surface temperature and precipitation response

In the $5BC_{1d}$ scenario, our model simulations show a net radiative imbalance at the surface of about –8 Wm^{-2} for about 5-6 months and then reduced to about –4 Wm^{-2} after 12 months relative to the reference case (Figure 2b, Table 2). The subsequently simulated global cooling at the surface ranges between 0.3 and 0.5°C over the year (Fig. 2c, Table 2). Such changes (radiative imbalance and cooling) are between two and three times smaller compared to previous studies (cf. for example Fig. 1 to Fig. 3 in Robock et al. 2007). As mentioned above, such a difference may be related to several aspects such as the different vertical and horizontal model resolution, the height of top of the model, the size of the emission region as well as the transport and dispersion of particles. Furthermore, compared to the study by *Mills et al.* [2014], the change in ocean temperature is substantially

smaller in our study (cf. Fig. 2d and Fig. 6 in *Mills et al.* [2014]), indicating that the ocean model may also play an important part in explaining the different results. When including the POM emissions in the 1 day and 1 month cases, a larger cooling of up to 1.3 °C is obtained during the first year (Fig. 2c, Table 2).

The 1 day and 1 week scenarios present somewhat similar global cooling in both the BC-only and BC/POM cases (Fig. 2c). On the other hand, the 1-month scenarios lead to a smaller cooling compared to the 1 day and 1 week scenarios (Fig 2c, Table 2). Without 45 Tg POM (i.e. $5BC_{1m}$), the surface temperature change is not significant compared to the internal variability in the model (Fig. 2c,d). Interestingly, in the 1-month scenarios, the net radiative imbalance at the surface is the largest during the first months after the release while at the end of the analyzed period they are, as expected, the smallest compared to the other scenarios (Fig. 2b).

In the $5BC_{1d}$ case, the mean global precipitation as well as cloud cover decreases compared to the reference climate (Figure 2e-f), which is consistent with earlier studies [*Robock et al.*, 2007; *Mills et al.*, 2014]. However, given the smaller radiative imbalance simulated in our model and the consequently much weaker cooling of the ocean compared to the above-mentioned studies, the magnitude of the decrease in global precipitation is about half of what was found in earlier experiments for the first year (cf. Fig. 2e and Figure 3d in *Mills et al.* [2014]).

Interestingly, while for temperature, the shorter-emission duration (1 day and 1 week) scenarios show the greatest globally averaged anomalies (Fig. 2c, d), for precipitation the 1-month scenarios display the largest impacts with a decrease of up to 50% more (Fig. 2e). The explanation for this sensitivity to emission duration is partly the horizontal and vertical dispersion of the particles and partly the effect that tropospheric aerosols may have on cloud properties and precipitation. For the 1-month emission scenarios, a larger fraction of the particles stay in the troposphere compared to the other scenarios as the maximum BC concentrations, and thus lofting, is lower (Fig. 1). The relatively higher concentration of aerosol particles in the higher troposphere (Fig. 1) increases the warming and thus also the tropospheric stability, which could reduce the precipitation. After

emission, the particles first spread around the emission latitude while lofted. Next, the particles are captured in the Northern Hemisphere (NH) mid-latitude circulation that result in lower temperatures all over the NH especially over land (see Fig. 3a, c, e and g for the reference case). The widespread cooling that takes place especially in the NH, is associated with a southern shift of the Intertropical Convergence Zone (ITCZ) and a significant weakening of the Indian Summer Monsoon (ISM) (Figs. 4 and 5). The interhemispherically asymmetric cooling pushes the ITCZ southwards [*Kang et al.*, 2008; *Schneider et al.*, 2014], leading to a weakening of the trade winds over the Tropical Pacific Ocean and consequently triggering an El Niño-like response [*Pausata et al.*, 2015b, 2016]. The cooling of sea surface temperatures and the southward shift of the ITCZ in combination with the heating of the troposphere by the BC, which stabilizes the atmospheric column over the Indian Ocean, are likely to be responsible for the weakening of the Indian Summer Monsoon (Fig. 5), as also shown in previous modeling studies (e.g., *Robock et al.* [2007]). These anomaly patterns are consistent among the different sensitivity experiments (Figs 3, 4 and 5); however, the most intense changes take place when both BC and POM are considered (Fig. 5), given the largest cooling obtained when including POM aerosols.

Summarizing, the strongest cooling occurs in the short-release-time scenarios, which is likely related to the enhanced lifting of the particles compared to the 1-month scenarios (Fig. 1 and 2c, Table 2). On the other hand, the strongest decrease in precipitation takes place in the long-release-time scenarios, which may be related to the larger tropospheric burden of particles (Fig. 1) caused by lower concentrations and less lifting of the BC/POM particles tropospheric stability and large-scale circulation patterns. The global mean cloud cover is however not the most affected in the 1-month scenarios (Fig. 2f), suggesting that the added particles in the troposphere lead to an increase in lifetime of the clouds and a decrease in precipitation (Fig. 2e). The understanding of these complex links is outside the scope of the present study.

3.3 Long term impacts on surface climate and growing season

To investigate the long term impacts of the BC/POM injection on climate and compared to previous

studies where only BC was considered, we extended the simulation with the intermediate BC/POM ratio and emission length (5BC/15POM$_{1w}$) to 10 years. We have chosen the intermediate scenarios because it is less extreme and hence possibly more plausible.

Our results show a slow decrease in the injected particles mass burden with an e-folding time of about 4 years (Fig. 6a), which is about half the time found in the BC-only scenario reported by Mills et al. [2014]. The net radiative flux perturbation at the surface peaks during the first year (Table 2), and then slowly approaches zero towards the end of the simulations (Fig. 6b). The surface cooling, on the other hand, peaks during the third year with a global cooling of about 1°C during the third year with a global cooling of about 1°C, but also approaches the range of internal variability towards the end of the simulation (Fig. 6c). In Mills et al. [2014] the temperature drops up to 2°C during the fifth year following the bomb detonation and a significant cooling (about 0.4°C) is still present after 20 years. Finally, the maximum decrease in global precipitation already occurs in the first year (~-0.2 mm/day, Fig. 6e) although the liquid water path has little change (Fig. 6f). The precipitation, however, starts recovering after the fourth year (Fig. 6e). The maximum decrease in precipitation is very similar to Mills et al. [2014]; however, the recovery time for the precipitation anomaly is also much longer in their simulations. The reason for the longer recovery time is the notably longer atmospheric residence time of the particles when they are lifted into the mesosphere.

The summer cooling of the NH continents strongly affects agriculture owing to the shortening of the growing season lasting several years after the bomb detonation. In the 5BC/5POM$_{1w}$ scenario, the length of the growing season, defined as the number of consecutive frost-free days, is shortened by 20 to 60 days and locally even longer (Fig. 7), peaking on the third year when the maximum cooling occurs. A similar decrease in the length of the growing season is reported in *Robock et al.* [2007].

Our analysis takes as a reference year 1986, when the global warming was less than present. Therefore, in the event a regional war happens in the future under severe global warming scenario,

the impacts on the shortening of the growing season will likely be reduced.

4 Discussion and Conclusions

In this study, we revisit the potential climate impacts of a hypothetical regional nuclear war placed over India and Pakistan, investigating the hitherto unexplored importance of the duration of the emissions, the amount of BC emitted and the sensitivity to adding POM (OC = ~POM/2) to the emissions.

In general, our model simulations confirm the results of previous studies [*Robock et al.*, 2007; *Toon et al.*, 2007b] on the large cooling in the year of the bomb detonation when making the same assumptions regarding initial conditions. However, our results point out that the magnitude of the simulated cooling is very sensitive to the assumptions made of the amount and type of particles emitted in the fires following the nuclear detonations as well as the duration of the emissions. The simulated range of cooling goes from a non-significant decrease in global mean temperature in the case of 5 Tg of BC emitted over a 30 day period to almost 1.5°C cooling by the end of the first year when both BC (5 Tg) and POM (45 Tg) are emitted in 1 day. The simulated cooling in our study is likely underestimated due to the limitation of our model which has a lower top (~45 km) compared to previous studies where it extends up to ~145 km [*Mills et al.*, 2014], and therefore limiting the lofting of the BC and POM. In contrast to temperature, the effects on precipitation are larger as the length of the emission increases. This suggests a key role played by the added particles (especially the POM) through aerosol-cloud interactions, which affects the life cycle of clouds. When the duration of the emissions is longer, a larger fraction of the released particles stay in the troposphere and thereby, increasing the effect on the clouds.

Another important aspect of POM injection is that POM limits the lofting to the upper stratosphere/mesosphere as shown in previous studies where only BC were considered. The reason is that that POM and BC can coagulate which increases the particle size (in particular at high concentrations – as when emissions occur over only 1 day or 1 week) and reduces the aerosol residence time. As a consequence, while our results still show long lasting climate effects (5-10

years), they substantially reduced compared to previous studies, in particular in Mills et al. [2014], where the surface cooling lasts for over 20 years.

Our results highlight the large cooling following a regional nuclear war that is most intense over the NH. The decrease in temperature is associated with a southward shift of the ITCZ as a response to the asymmetric cooling between NH and SH [*Kang et al.*, 2008]. This equatorward ITCZ shift implies a weakening of the easterly winds along the equator in the central and eastern equatorial Pacific, since surface easterly winds are weakest under the ITCZ. This leads via the Bjerknes feedback [*Bjerknes*, 1969] to a reduction in the east-west temperature contrast across the tropical Pacific, thus favoring an El Niño-like anomaly. This mechanism is similar to what has been shown to occur after large high-latitude volcanic eruptions by *Pausata et al.* [2015a]. The NH cooling is also associated to a decreased strength in the monsoon systems, especially the Indian Summer Monsoon, and a widespread reduction in the growing season in the NH, locally up to two months.

Finally, the difference between the only BC and BC/POM scenarios may be slightly less pronounced because our model does not include the ozone chemistry. Ozone may react with POM in the stratosphere which could modify the absorption properties of the POM as well as the total aerosol mass. In addition, previous estimates of ozone loss for a regional nuclear war [*Mills et al.*, 2008] are, however, likely underestimated because they did not include the further ozone depletion induced by the presence of POM, but only considered the increased ozone reaction rate caused by the large stratospheric warming.

In summary, our study highlights some crucial aspects that need to be taken into account in future studies for a more in-depth understanding of the climatic consequence associated with a regional nuclear war: the temporal extent of the fires, the amount and type of particles emitted, their radiative properties, and the cloud-particles interactions. Our results suggest that the cooling and the precipitation changes associated with a regional nuclear strongly depend on the choice of the emission type, amount and the duration. Our study also suggests that the extremely long-term

cooling (>20 years) proposed in previous studies might be notably shortened in a case with POM injection and longer emission duration. The POM injection and the increased emission duration confine the aerosol particles to lower heights.

Furthermore, recent studies [*Gleckler et al.*, 2006; *Stenchikov et al.*, 2009; *Pausata et al.*, 2015b; *Swingedouw et al.*, 2015] have shown that the large surface cooling induced by the volcanic eruption alters the ocean circulation and the ocean heat content for decades. Therefore more in-depth studies with a larger ensemble of high-resolution and high-top fully coupled climate model simulations are warranted in order to better constrain the disastrous global climate impacts of even a limited regional nuclear war using a very small fraction (less than 1%) of the global arsenal of nuclear weapons. In addition, further studies on fire characteristics, estimating the burnable material available in different countries will be necessary to better represent the BC/POM ratio, are also necessary to better constrain the impact of a potential regional nuclear war on climate.

Acknowledgment. The authors would like to thank two anonymous reviewers, O. Brian Toon and Alan Robock for discussions and comments on the manuscript, and Bob Yokelson for insightful suggestions. Data used in this paper may be obtained upon request to J.L. (jenny.lindvall@misu.su.se).

References

Assmann, K. M., M. Bentsen, J. Segschneider, and C. Heinze (2010), Model Development An isopycnic ocean carbon cycle model, *Geosci. Model Dev.*, *3*, 143–167.

Bentsen, M. et al. (2013), The Norwegian Earth System Model, NorESM1-M – Part 1: Description and basic evaluation of the physical climate, *Geosci. Model Dev.*, *6*(3), 687–720, doi:10.5194/gmd-6-687-2013.

Bjerknes, J. (1969), Atmospheric teleconnections from the equatorial Pacific, *Mon. Weather Rev.*, *97*(3), 163–172, doi:10.1175/1520-0493(1969)097<0163:ATFTEP>2.3.CO;2.

Bond, T. C., D. Streets, K. F. Yarber, S. M. Nelson, J.-H. Woo, and Z. Klimont (2004), A technology-based global inventory of black and organic carbon emissions from combustion, *J. Geophys. Res.*, *109*(D14), D14203, doi:10.1029/2003JD003697.

Gent, P. R. et al. (2011), The Community Climate System Model Version 4, *J. Clim.*, *24*(19), 4973–4991, doi:10.1175/2011JCLI4083.1.

Gleckler, P. J., T. M. L. Wigley, B. D. Santer, J. M. Gregory, K. Achutarao, and K. E. Taylor (2006), Volcanoes and climate: Krakatoa's signature persists in the ocean., *Nature*, *439*(7077), 675, doi:10.1038/439675a.

Iversen, T. et al. (2013), The Norwegian Earth System Model, NorESM1-M – Part 2: Climate response and scenario projections, *Geosci. Model Dev.*, *6*(2), 389–415, doi:10.5194/gmd-6-389-2013.

Kang, S. M., I. M. Held, D. M. W. Frierson, and M. Zhao (2008), The Response of the ITCZ to Extratropical Thermal Forcing: Idealized Slab-Ocean Experiments with a GCM, *J. Clim.*, *21*(14), 3521–3532, doi:10.1175/2007JCLI2146.1.

Kirkevåg, A. et al. (2013), Aerosol-climate interactions in the Norwegian Earth System Model - NorESM1-M, *Geosci. Model Dev.*, *6*, 207–244, doi:10.5194/gmd-6-207-2013.

Liu, Y., S. Goodrick, and W. Heilman (2014), Wildland fire emissions, carbon, and climate: Wildfire–climate interactions, *For. Ecol. Manage.*, *317*, 80–96, doi:10.1016/j.foreco.2013.02.020.

May, A. A. et al. (2014), Aerosol emissions from prescribed fires in the United States: A synthesis of laboratory and aircraft measurements, *J. Geophys. Res. Atmos.*, *119*(20), 11,826–11,849, doi:10.1002/2014JD021848.

Mills, M. J., O. B. Toon, R. P. Turco, D. E. Kinnison, and R. R. Garcia (2008), Massive global ozone loss predicted following regional nuclear conflict., *Proc. Natl. Acad. Sci. U. S. A.*, *105*(14), 5307–12, doi:10.1073/pnas.0710058105.

Mills, M. J., O. B. Toon, J. Lee-Taylor, and A. Robock (2014), Multidecadal global cooling and unprecedented ozone loss following a regional nuclear conflict, *Earth's Futur.*, *2*(4), 161–176, doi:10.1002/2013EF000205.

Neale, R. B., J. Richter, S. Park, P. H. Lauritzen, S. J. Vavrus, P. J. Rasch, and M. Zhang (2013), The Mean Climate of the Community Atmosphere Model (CAM4) in Forced SST and Fully Coupled Experiments, *J. Clim.*, *26*(14), 5150–5168, doi:10.1175/JCLI-D-12-00236.1.

Özdoğan, M., A. Robock, and C. J. Kucharik (2013), Impacts of a nuclear war in South Asia on soybean and maize production in the Midwest United States, *Clim. Change*, *116*(2), 373–387, doi:10.1007/s10584-012-0518-1.

Pausata, F. S. R., A. Grini, R. Caballero, A. Hannachi, and Ø. Seland (2015a), High-latitude volcanic eruptions in the Norwegian Earth System Model: the effect of different initial conditions and of the ensemble size, *Tellus B*, *67*(26728).

Pausata, F. S. R., L. Chafik, R. Caballero, and D. S. Battisti (2015b), Impacts of high-latitude volcanic eruptions on ENSO and AMOC, *Proc. Natl. Acad. Sci.*, 201509153, doi:10.1073/pnas.1509153112.

Pausata, F. S. R., C. Karamperidou, R. Caballero, and D. S. Battisti (2016), ENSO response to high-latitude volcanic eruptions in the Northern Hemisphere: The role of the initial conditions, *Geophys. Res. Lett.*, *43*(16), 8694–8702, doi:10.1002/2016GL069575.

Robock, A., L. Oman, G. L. Stenchikov, O. B. Toon, C. Bardeen, and R. P. Turco (2007), Climatic consequences of regional nuclear conflicts, *Atmos. Chem. Phys.*, *7*(8), 2003–2012, doi:10.5194/acp-7-2003-2007.

Schneider, T., T. Bischoff, and G. H. Haug (2014), Migrations and dynamics of the intertropical convergence zone., *Nature*, *513*(7516), 45–53, doi:10.1038/nature13636.

Stenchikov, G., T. L. Delworth, V. Ramaswamy, R. J. Stouffer, A. Wittenberg, and F. Zeng (2009), Volcanic signals in oceans, *J. Geophys. Res.*, *114*(D16), D16104, doi:10.1029/2008JD011673.

Stenke, A., C. R. Hoyle, B. Luo, E. Rozanov, J. Gröbner, L. Maag, S. Brönnimann, and T. Peter (2013), Climate and chemistry effects of a regional scale nuclear conflict, *Atmos. Chem. Phys.*, *13*(19), 9713–9729, doi:10.5194/acp-13-9713-2013.

Swingedouw, D., P. Ortega, J. Mignot, E. Guilyardi, V. Masson-Delmotte, P. G. Butler, M. Khodri, and R. Séférian (2015), Bidecadal North Atlantic ocean circulation variability controlled by

timing of volcanic eruptions., *Nat. Commun.*, *6*, 6545, doi:10.1038/ncomms7545.

Toon, O. B., and T. P. Ackerman (1981), Algorithms for the calculation of scattering by stratified spheres., *Appl. Opt.*, *20*(20), 3657–60, doi:10.1364/AO.20.003657.

Toon, O. B., and N. H. Farlow (1981), Particles Above the Tropopause: Measurements and Models of Stratospheric Aerosols, Meteoric Debris, Nacreous Clouds, and Noctilucent Clouds, *Annu. Rev. Earth Planet. Sci.*, *9*(1), 19–58, doi:10.1146/annurev.ea.09.050181.000315.

Toon, O. B., R. P. Turco, A. Robock, C. Bardeen, L. Oman, and G. L. Stenchikov (2007a), Atmospheric effects and societal consequences of regional scale nuclear conflicts and acts of individual nuclear terrorism, *Atmos. Chem. Phys.*, *7*(8), 1973–2002, doi:10.5194/acp-7-1973-2007.

Toon, O. B., A. Robock, R. P. Turco, C. Bardeen, L. Oman, and G. L. Stenchikov (2007b), Nuclear war. Consequences of regional-scale nuclear conflicts., *Science*, *315*(5816), 1224–5, doi:10.1126/science.1137747.

Turco, R. P., O. B. Toon, T. P. Ackerman, J. B. Pollack, and C. Sagan (1983), Nuclear winter: global consequences of multple nuclear explosions., *Science*, *222*(4630), 1283–92, doi:10.1126/science.222.4630.1283.

Turpin, B. J., and H.-J. Lim (2001), Species Contributions to PM2.5 Mass Concentrations: Revisiting Common Assumptions for Estimating Organic Mass, *Aerosol Sci. Technol.*, *35*, 602–610.

Xia, L., and A. Robock (2013), Impacts of a nuclear war in South Asia on rice production in Mainland China, *Clim. Change*, *116*(2), 357–372, doi:10.1007/s10584-012-0475-8.

Xia, L., A. Robock, M. Mills, A. Stenke, and I. Helfand (2015), Decadal reduction of Chinese agriculture after a regional nuclear war, *Earth's Futur.*, *3*(2), 37–48, doi:10.1002/2014EF000283.

Table 1: Details of the model experiments. Injection location is over land regions only.

Experiment name	Emission BC (Tg)	Emission POM (Tg)	Emission duration	# Ensemble members	Injection location
$5BC_{1d}$	5	0	1 day	10	9-29°N 70-88°E 300-150 hPa
$5BC_{1w}$	5	0	1 week	10	
$5BC_{1m}$	5	0	1 month	10	
$5BC/15POM_{1d}$	5	15	1 day	10	
$5BC/15POM_{1w}$	5	15	1 week	10	
$5BC/15POM_{1m}$	5	15	1 month	10	
$5BC/45POM_{1d}$	5	45	1 day	5	
$5BC/45POM_{1w}$	5	45	1 week	5	
$5BC/45POM_{1m}$	5	45	1 month	5	

Table 2: Maximum change of globally averaged monthly mean surface parameters in the first year after the bomb detonation: Net change in radiative flux at the surface (ΔRF), in surface temperature (ΔT_{sfc}) and precipitation (ΔPRECT).

Experiment name	ΔRF (Wm^{-2})	ΔT_{sfc} (^oC)	ΔPRECT ($mm\ day^{-1}$)
$5BC_{1d}$	–8.2	–0.48	–0.14
$5BC_{1w}$	–9.2	–0.45	–0.19
$5BC_{1m}$	–10.0	–0.12	–0.19
$5BC/15POM_{1d}$	-10.6	-0.88	-0.18
$5BC/15POM_{1w}$	-12.0	-0.71	-0.20
$5BC/15POM_{1m}$	-13.5	-0.32	-0.21
$5BC/45POM_{1d}$	–15.2	–1.3	–0.20
$5BC/45POM_{1w}$	–17.6	–1.1	–0.24
$5BC/45POM_{1m}$	–18.8	–0.75	–0.28

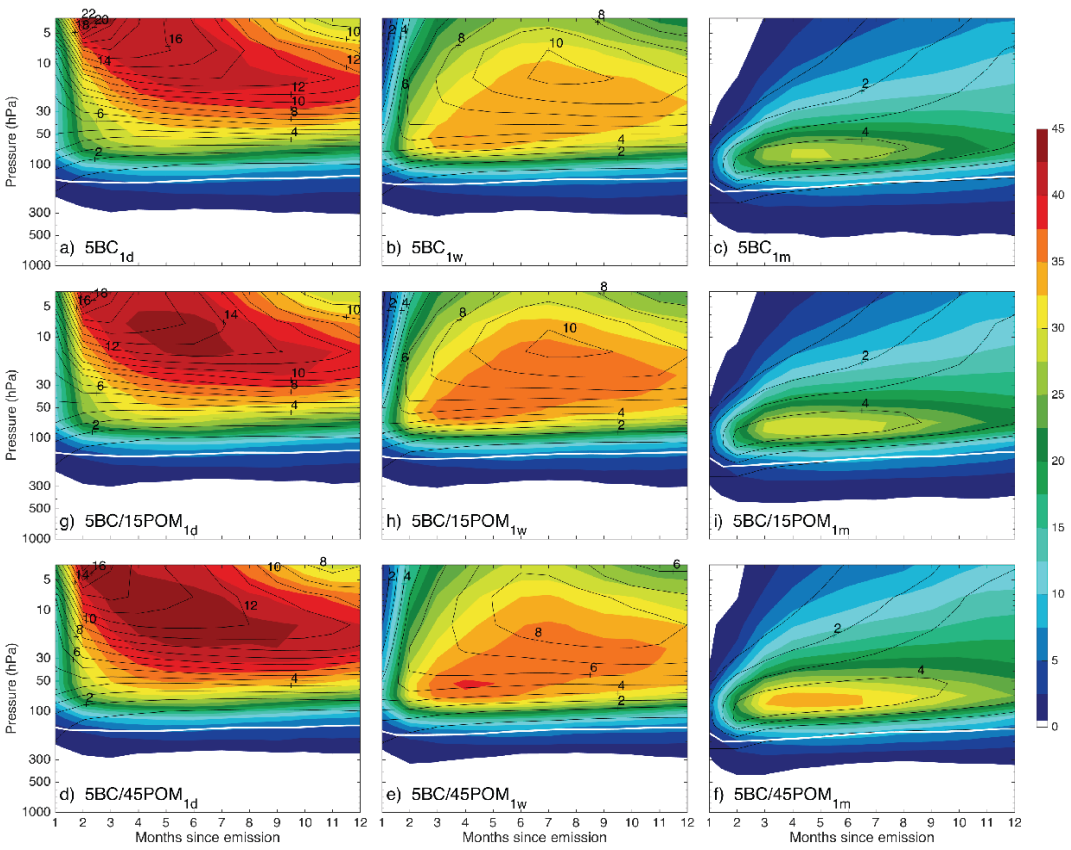

Figure 1: Vertical profile of mean temperature (color shadings, °C) and black carbon mixing ratio (black contours, µg/m^3) anomaly relative to the reference ensemble averaged over the entire globe for each month following the bomb detonation and for each scenario. The white line delimitates the zonal mean tropopause height at 20°N. In the BC+POM experiments, we have shown only the BC mixing ratio to ease the comparison with the BC cases. The POM mixing ratios follow the same behavior as the BC mixing ratios (not shown).

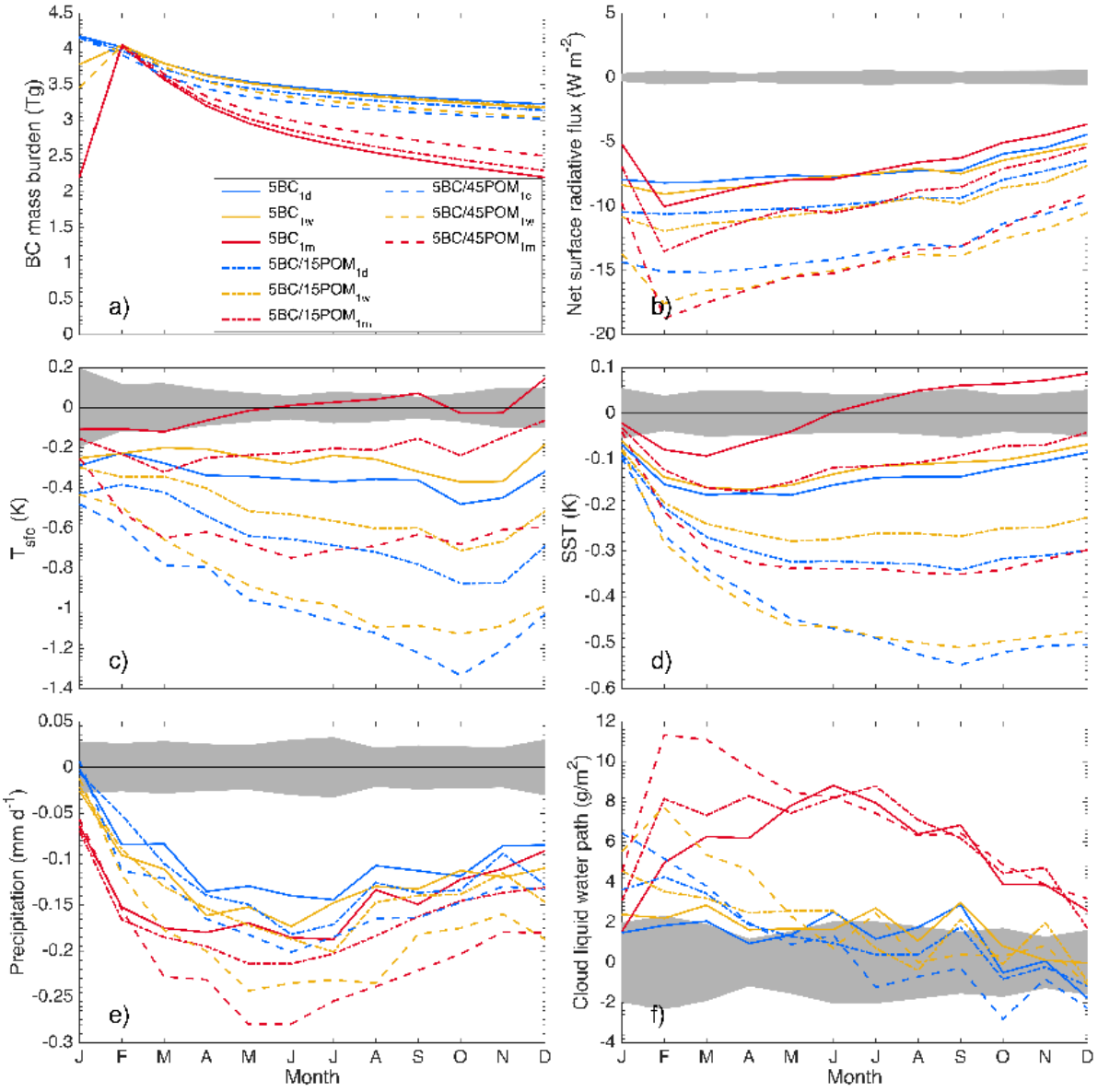

Figure 2: Globally averaged monthly mean anomalies relative to the reference ensemble of a) BC mass burden, b) Net surface radiative flux, c) surface temperature, d) sea surface temperature, e) precipitation and f) cloud liquid water path for each month following the bomb detonation and for each scenario. The gray shadings show the confidence intervals in which the difference relative to the reference scenario is not significant at 95% confidence level.

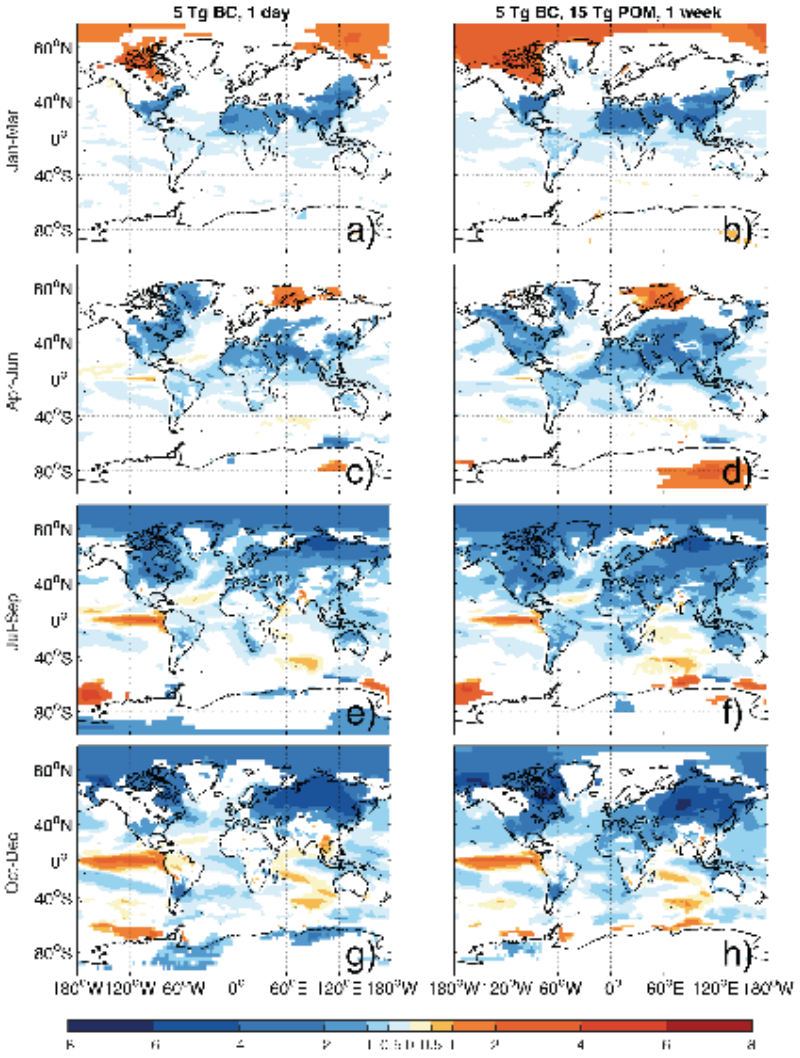

Figure 3: Changes in surface temperature (°C) between 5 Tg BC released during one day ($5BC_{1d}$, left panels) and 5 Tg BC + 15 Tg POM released during one week ($5BC/15POM_{1w}$, right panels), and the reference simulation for four seasons. Only changes significant at 95% confidence level using a *t* test are shown.

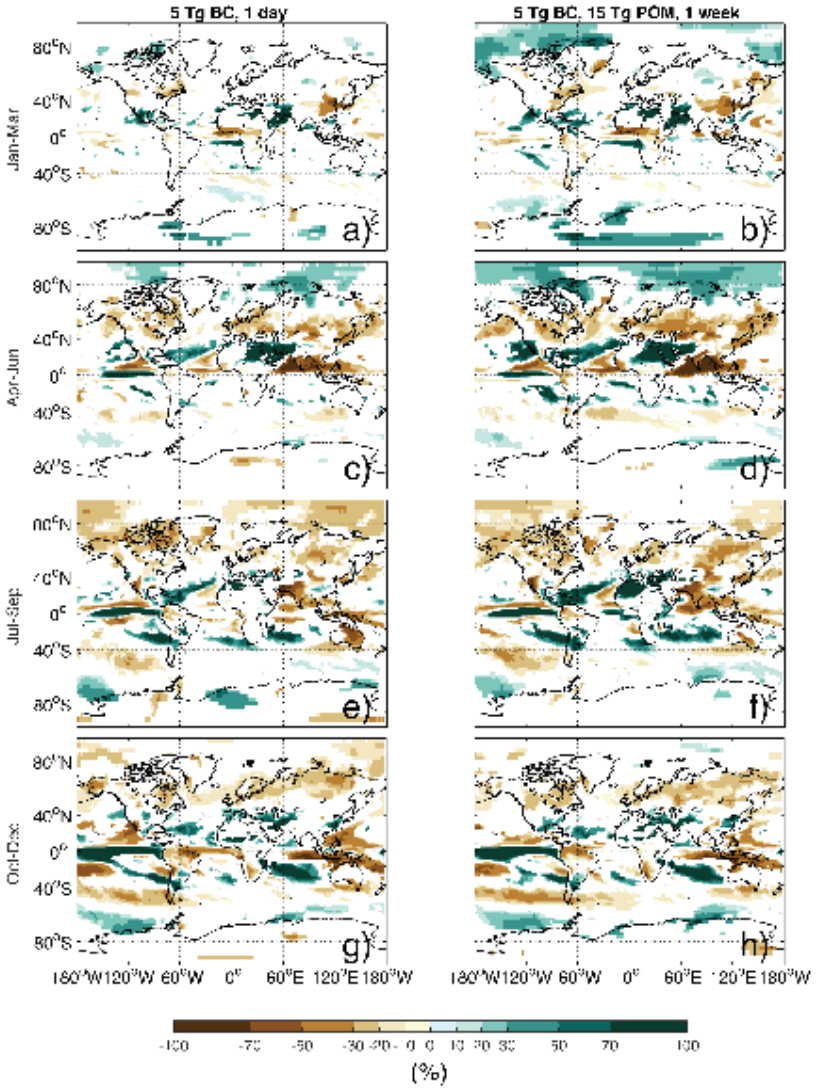

Figure 4: Changes in precipitation (%) between 5 Tg BC released during one day ($5BC_{1d}$, left panels) and 5 Tg BC + 15 Tg POM released during one week ($5BC/15POM_{1w}$, right panels), and the reference simulation for four seasons. Only changes significant at 95% confidence level using a *t* test are shown.

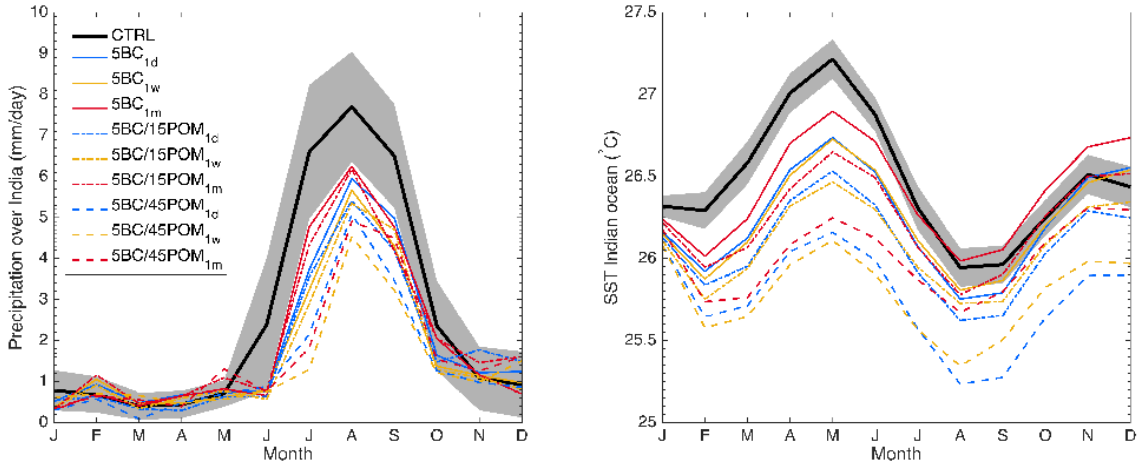

Figure 5: Annual cycle of monthly average Indian Ocean SST (right) and precipitation over India and Pakistan (left) for each month following the bomb detonation and for each scenario. The gray shadings show the confidence intervals in which the difference relative to the reference scenario is not significant at 95% confidence level.

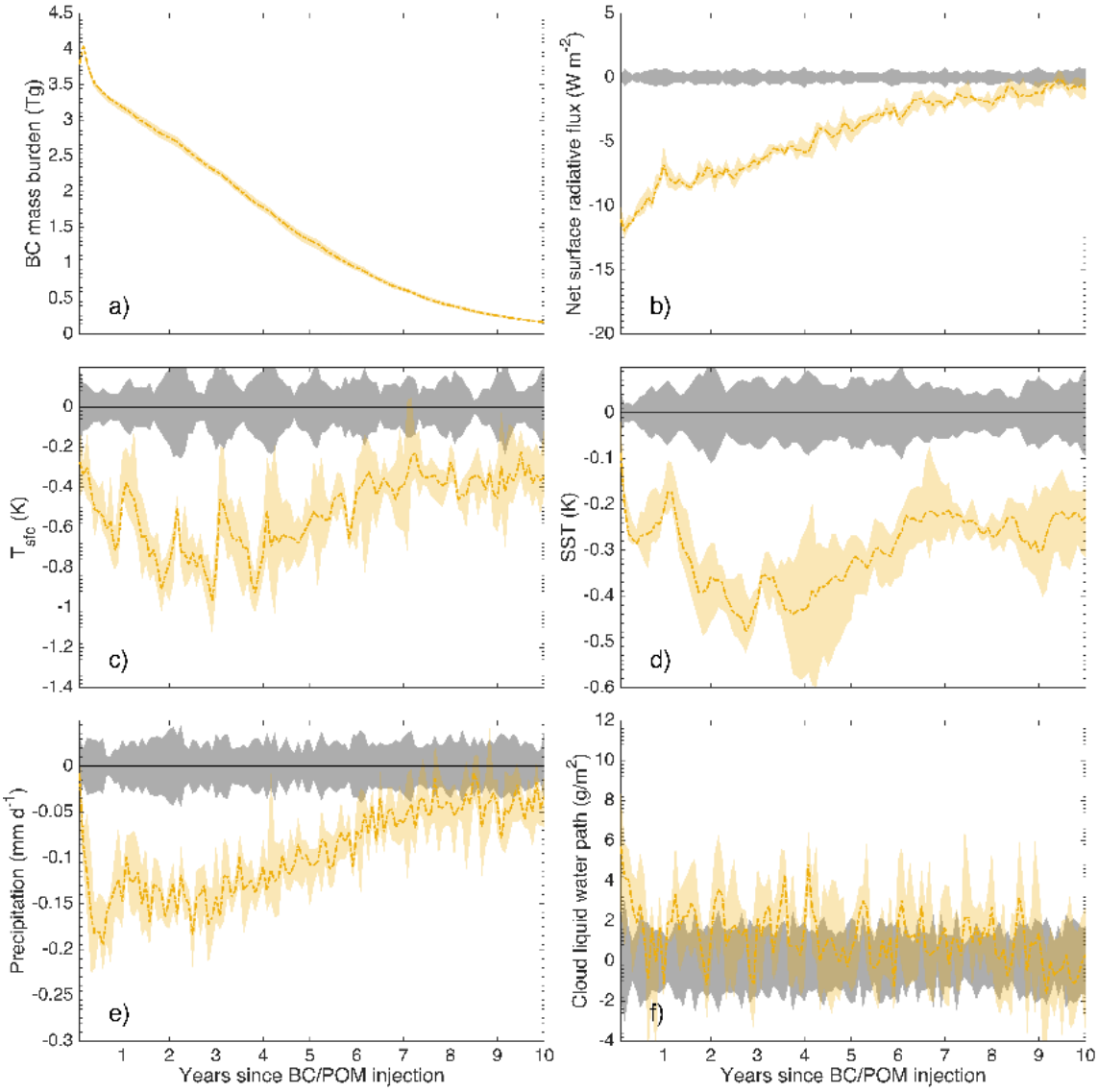

Figure 6: Changes in surface temperature (°C) between 5 Tg BC released during one day ($5BC_{1d}$, left panels) and 5 Tg BC + 45 Tg POM released during one week ($5BC/45POM_{1w}$, right panels), and the reference simulation for four seasons. Only changes significant at 95% confidence level using a *t* test are shown.

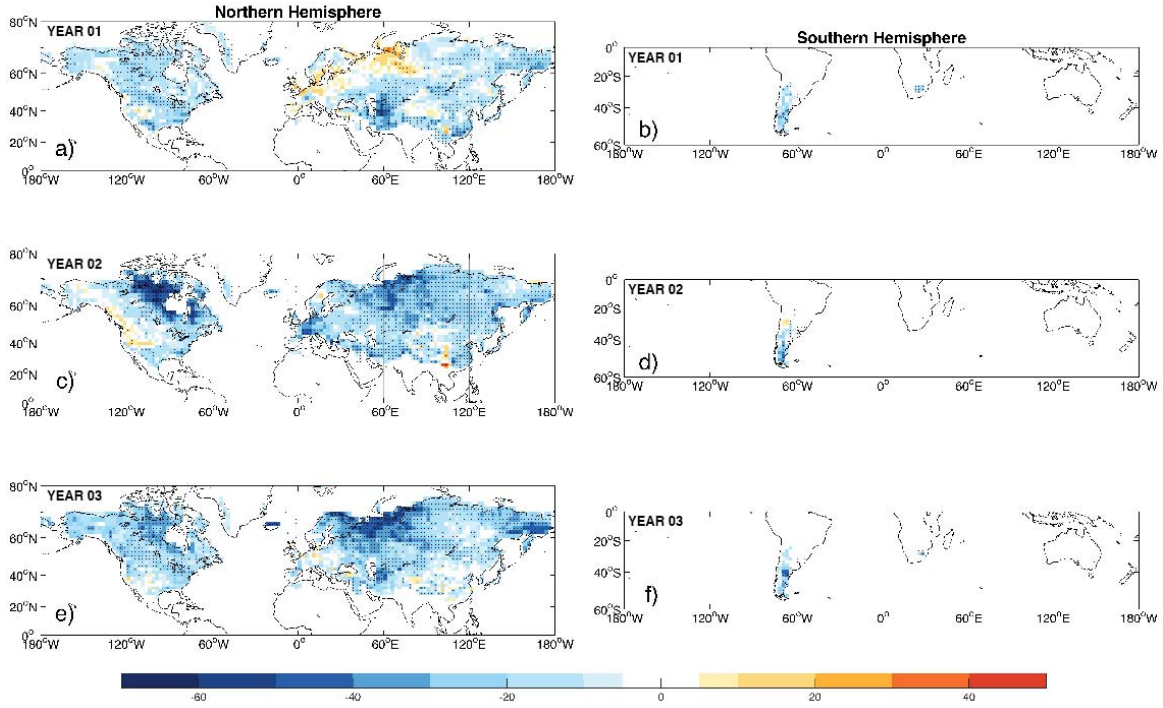

Figure 7: Change in the length of the growing season for the first three years following the bombs' detonation in the 5 Tg BC + 15 Tg POM released during one week ($5BC/15POM_{1w}$) relative to the reference simulation for the Northern and Southern Hemisphere. The length of the growing season has been defined as the length of frost-free days over the Northern Hemisphere. Regions where changes are significant at 95% confidence level using a *t* test are stippled.